Chemical Science

ROYAL SOCIETY OF CHEMISTRY

EDGE ARTICLE

View Article Online
View Journal | View Issue

Cite this: *Chem. Sci.*, 2025, **16**, 15265

All publication charges for this article have been paid for by the Royal Society of Chemistry

Received 9th May 2025
Accepted 16th July 2025

DOI: 10.1039/d5sc03378k

rsc.li/chemical-science

Detection and characterization of a compound 1 species from the *c*-type heme enzyme cytochrome c'_β†

Jared C. Paris, [a] Joline Nguyen,‡[b] Hyung J. Kim [b] and Michael P. Hendrich *[a]

Compound **1** is a key intermediate in a large group of enzymes containing heme *b* including cytochromes (cyt) P450, peroxidases and catalases. The extreme reactivity of this highly oxidized species has made its trapping and characterization challenging. Cyt c'_β of the ammonia-oxidizing bacterium *Nitrosomonas europaea* is an enzyme containing heme *c* and a member of the P460 superfamily of cytochromes. Herein, a compound **1** species within the P460 superfamily was trapped and spectroscopically characterized with stopped-flow absorption, EPR and variable-field Mössbauer spectroscopy. Like horseradish peroxidase (HRP), Cyt c'_β has an axial His coordinated to the heme iron with the compound **1** species exhibiting a green color with an absorption spectrum similar to that of HRP. Compound **1** from Cyt c'_β features an antiferromagnetic exchange coupling between an $S = 1$ iron(IV)-oxo center and an $S = \frac{1}{2}$ porphyrin radical, but with an exchange coupling constant that is significantly greater than that for HRP. The large variation in the exchange constant for both enzymes, despite both having the same axial ligand, indicates that this value is not strongly correlated to the axial ligand identity. Although the reaction of Cyt c'_β with H_2O_2 was found to be significantly slower than other peroxidases, the lifetime of the compound **1** species was comparable to other heme enzymes that oxidize a variety of substrates, suggesting that the *in vivo* function of cyt c'_β may not be relegated solely to the clearance of H_2O_2. Given its presence in an ammonia-oxidizing bacterium, cyt c'_β could oxidize nitrogen containing substrates.

Introduction

The reaction of heme containing peroxidases with peroxide compounds has long been known to produce transient, highly oxidized iron porphyrin species that function as powerful biological oxidants.[1–3] The primary intermediate, referred to as compound **1**, is 2-oxidation equivalents above the resting ferric oxidation state, and composed of a ferryl (Fe^{IV}=O) center and a porphyrin radical which gives the heme a green color. This is the cofactor state following heterolytic scission of the O–O bond of the iron bound peroxide; it is highly reactive, difficult to isolate, and serves as the catalytic intermediate for many difficult oxidative reactions in nature. Reduction of compound **1** by one electron from a nearby amino acid residue or substrate produces compound **2**, which has a similar iron center as compound **1**, but with the porphyrin radical being reduced, resulting in a heme that is red in color. Historically, the primary intermediate compound **1** species have been characterized in cytochromes bearing heme *b*, namely P450s, peroxidases and catalases. However, no compound **1** species from enzymes containing heme *c* have been kinetically characterized.

Cytochromes with heme *c* are distinguished from those with heme *b* by the heme-protein interaction. Cytochromes with heme *b* have their heme linked to the protein *via* the coordination of the axial amino acid side chain to the heme iron (*e.g.*, S-Cys for cyt P450s, N-His for peroxidases, and O-Tyr for catalases).[1] Besides the hydrophobic and polar interactions between the heme and the protein common in all heme-protein complexes,[4] the coordination of the axial ligand to the heme iron is the only covalent linkage in cytochromes with heme *b*. This linkage influences the overall electronic structure of heme ferryl intermediates which in turn affects function. Green compound **1** species have an Fe^{IV}=O center with an intermediate spin $S_{Fe} = 1$ coupled to a porphyrin π-orbital unpaired spin ($S_{Por} = 1/2$); the net spin is described by the exchange coupling parameter (J, $H_{ex} = JS_1 \cdot S_2$) which has been observed to be correlated with the heme axial ligand. The value of J based on EPR and Mössbauer observations is antiferromagnetic ($J > 0$) for cyt P450s, near zero for peroxidases, and ferromagnetic ($J < 0$) for catalases.[5–7] Although all three proteins generate compound **1**, they are not equivalent mechanistically, due at least in part to

[a]*Department of Chemistry, Carnegie Mellon University, 4400 Fifth Ave., Pittsburgh, PA, 15213, USA. E-mail: hendrich@andrew.cmu.edu*

[b]*Division of Physical Sciences, Chemistry, University of Washington Bothell, Bothell, Washington, 98012, USA*

† Electronic supplementary information (ESI) available. See DOI: https://doi.org/10.1039/d5sc03378k

‡ Present address: Department of Biochemistry & Biophysics, Oregon State University, Corvallis, OR, 97331, USA.

their axial ligands, surrounding residues, and electronic structures.

Cytochromes bearing heme *c* have additional linkages afforded by the amino acid sequence CXXCH heme binding motif where the two cysteine residues tether the heme *via* two thioether covalent bonds to the vinyl carbons of the porphyrin ring; the histidine residue in the motif coordinates to the heme iron (Fig. 1). Whether this difference in the heme-protein interaction influences the electronic structure of the compound **1** containing heme *c* has been unknown. We have characterized the one-electron oxidized Fe^{IV}=O species of the cytochrome c'_β (cyt c'_β) from the ammonia-oxidizing bacteria *Nitrosomonas europaea*.[8,9] Using optical and magnetic spectroscopy, we showed that a slight excess of H_2O_2 with manual mixing generated an optical spectrum indicative of compound **2**. Although a significantly diminished Soret band suggestive of a porphyrin radical (compound **1**) was observed prior to the compound **2** spectrum, EPR and Mössbauer analyses in the same time frame indicated an Fe^{IV}=O porphyrin structure lacking the porphyrin radical; instead, a small amount of an organic radical could be detected. Nevertheless, cyt c'_β showed peroxidase-like activity, albeit slow, with guaiacol, pyrogallol, and 2,2′-azino-bis(3-ethylbenzothiazoline-6-sulfonic acid.

N. europaea cyt c'_β is a 19 kDa cytochrome characterized by an unusual β-sheet fold, in contrast to most cytochromes which are helical, placing it in the "P460" family of cytochromes[10] that are present in bacteria that metabolize N-oxides (*e.g.* nitric oxide). The recent 1.8 Å crystal structure (Fig. 2A) revealed a 5-coordinate heme iron active site that possesses an Arg residue as the putative acid-base catalyst, replacing the conserved His–Arg pair in peroxidases (*e.g.* HRP, Fig. 2C).[8,11] Furthermore, the conserved Asp residue near the proximal His ligand of peroxidases critical to providing imidazolate character during compound **1** formation is absent. Rather, the negative charge could be provided by a heme propionate in cyt c'_β (Fig. 2A). Thus, our biochemical and structural data indicate that *c*-type hemes can generate ferryl intermediates, possibly with nuanced mechanistic and electronic variations compared to the ferryl species with heme *b*. This notion has broader implications to the widely distributed prototypical cytochrome with heme *c*, mitochondrial cytochrome *c* (cyt *c*), that shuttles electrons between two redox centers in electron transport chains (*e.g.*, *bc*1 complex and cytochrome *c* oxidase of mitochondria, bacteria, and plants). Mitochondrial cyt *c* gains peroxidase activity[12,13] under oxidative stress conditions leading to lipid peroxidation, downstream cell signaling, and cell apoptosis (programmed cell death). The conversion to a peroxidase is driven by a transition from a six-coordinate heme to a five-coordinate peroxidase-like system. This raises the question if enzymes with heme *c*, such as cyt *c*, readily accesses the compound **1** intermediate, despite structural differences in the way the heme is complexed to the protein.

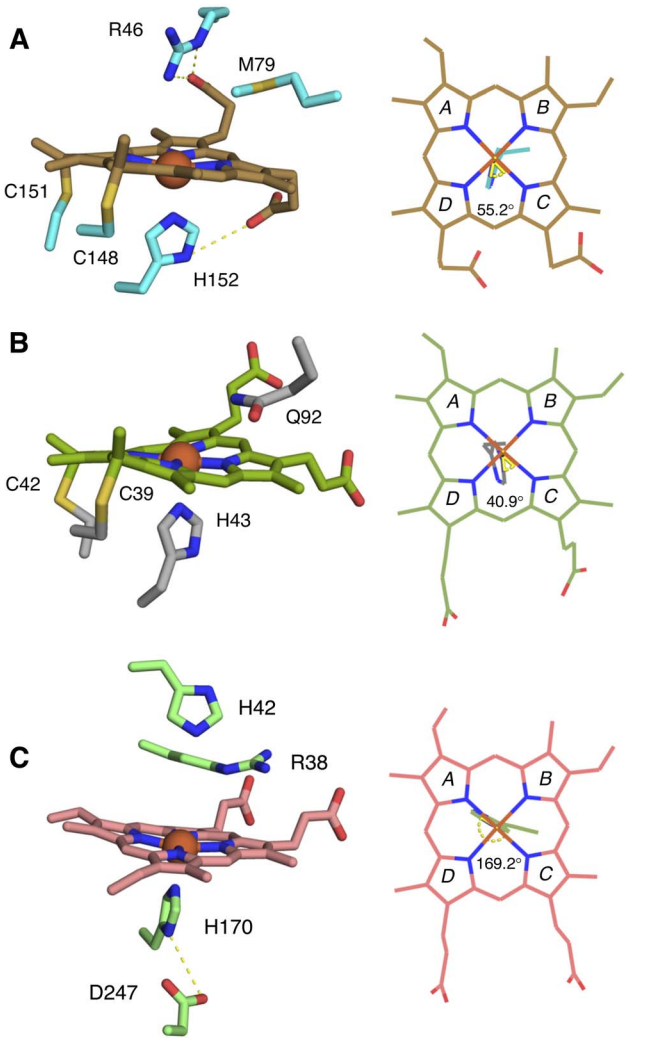

Fig. 2 The active-site structures of the resting ferric states of cyt c'_β (A, 7S5O), bCcP (B, 1IQC) and HRP (C, 1H5A).[8,11,14] The hemes are shown in similar orientations to highlight the roughly 90° rotation of the axial proximal His of the *c*-type hemes relative to the *b*-type heme of HRP. The highly conserved distal His170-Arg38 pair in HRP is replaced by an Arg46-Met79 pair in cyt c'_β in comparable positions. Additionally, the heme of cyt c'_β is distorted in a ruffled shape with a propionate hydrogen bonded to His152, which further differentiates its active site from that of peroxidases. Dashed lines indicate possible H-bond interactions. Figures to the right indicate the dihedral angle between the following two planes: the imidazole ring of the proximal His defined by Cε–Nε atoms relative to the plane defined by Fe–N (ring C) atoms of the of the porphyrin. The dihedral angle of cyt c'_β listed corresponds to chain A of the crystal structure. Angles for chains B and C are 57.5° and 58.5° respectively.

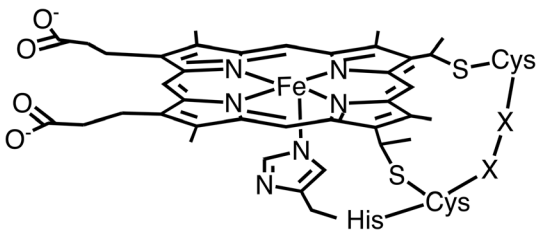

Fig. 1 Heme *c* structure in cytochromes. The CXXCH motif is shown where the cysteines covalently bond to the vinyl carbons of the porphyrin.

Here, using stopped-flow absorbance (SF-Abs) and rapid freeze quench (RFQ) methods with purified cyt c'_β, c'_β including ^{57}Fe-enriched preparations, we trap and characterize a green compound **1** intermediate from cyt c'_β. The kinetic rate constant for the reaction of cyt c'_β with H_2O_2 was found to be significantly slower than for other peroxidases, whereas the rate of decay of compound **1** was found to be comparable or slower than that of chloroperoxidase (CPO) and cyt P450. These rates suggest that the *in vivo* function of cyt c'_β may not be to detoxify H_2O_2 as in peroxidases or catalases, but could use compound **1** as a potent oxidant catalyst for the conversion of cellular substrates.

Very recently, a compound **1** intermediate has been spectroscopically characterized from a bacterial di-heme peroxidase (bCcP) containing hemes *c* also from *Nitrosomonas europaea*.[15] The heme structure from bCcP is shown in Fig. 2B for comparison.[14] The compound **1** intermediates of cyt c'_β and bCcP are the first known examples from heme *c*, although a ferryl intermediate is involved in cyt P460 cofactor maturation independent of compound **1**.[16] Here and in the bCcP paper, we determine the exchange coupling constants using Mössbauer spectroscopy. We show here that the values of *J* differ significantly between cyt c'_β bCcP and HRP even though all three have an axial His to the heme and otherwise similar electronic characteristics. Furthermore, the variation in the coupling constant cannot be attributed to heme *b versus* heme *c*. The values of *J* for cyt c'_β and bCcP are significantly positive and negative, respectively, implying that the sign change is not related to porphyrin radical delocalization onto the axial heme ligand.[17–21] This suggests that the porphyrin structure and/or its microenvironment is a dominant determinant of the exchange coupling constant, rather than the axial heme ligand or heme type.

Results

Stopped-flow absorbance (SF-Abs)

The absorption spectrum of ferric cyt c'_β displayed prominent absorbances at 397, 500, and 640 nm consistent with previous enzyme preparations (Fig. 3, initial red trace).[9] The pre-steady state kinetics of the peroxidase activity were monitored with SF-Abs during reactions of ferric cyt c'_β with either H_2O_2 or *meta*-chloroperoxybenzoic acid (mCPBA).

Rapid mixing of ferric cyt c'_β with a 20-fold excess of H_2O_2 gave significant changes in both the Soret and Q-bands of the ferric enzyme. During the time span of 0 to 3 s (Fig. 3A, red to green traces), three isosbestic points were observed at the wavelengths marked on Fig. 3, indicating the formation of a new species (species **1**) concomitantly with the loss of the ferric enzyme. The equal time interval spectra showed convergence to a species with red shifted absorbances at 404, 512, and 642 nm. The absorbances of species **1** (lower Soret intensity, red shift and growth of a 642 feature) are similar to previously characterized compound **1** type species (Table 1). In particular, the 642 nm feature are within the range (640 to 690 nm) of the green color attributed to the porphyrin π radical delocalized within the porphyrin ring of the compound **1** iron-oxo species.

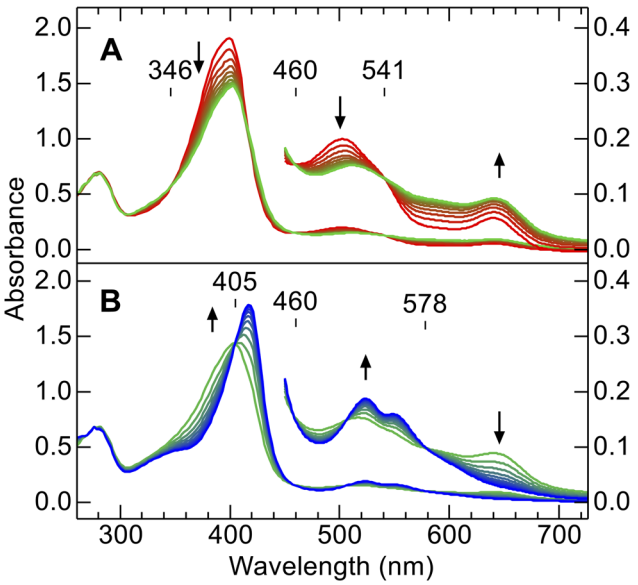

Fig. 3 Stopped-flow absorption spectra of resting c'_β (40 μM) reacting with excess H_2O_2 (800 μM) at 4 °C in the time regime of (A, red to green) 0 to 3 s and (B, green to blue) 5 to 50 s. The time interval between successive spectra is (A) 0.33 s and (B) 5 s. The insets are magnified by 5 and use the right-axis absorbance scale. The arrows indicate the increasing time changes and the denoted wavelengths are isosbestic points.

Table 1 Compound **1** optical bands of applicable of compound **1** species

	λ_{max}, nm, [ε, mM^{-1} cm^{-1}]		
	Soret	Q bands	Ref.
Cyt c'_β (H_2O_2)	404	512, 642	This work
Cyt c'_β (mCPBA)	400 [93]	586 [5], 645 [15]	This work
bCcP (H_2O_2)	409	658	15
HRP (H_2O_2)	402 [80]	580 [5], 640 [5]	22 and 23
HRP (mCPBA)	400	577, 622, 651	24
CPO (H_2O_2)	367 [49]	545 [7], 610 [6.5], 688 [11.7]	25
P450 (mCPBA)	370 [∼50]	610 [∼40], 690 [40]	26 and 27

Over a much longer time span of 5 to 50 s (Fig. 3B, green to blue traces), three new isosbestic points were observed at the wavelengths marked on the figure, indicating the formation of a new species (species **2**) concomitantly with the loss of species **1**. The equal time interval spectra showed convergence to a species with a further red shifted Soret band at 417 nm, Q-bands at 524 and 551 nm, and the loss of the 642 nm absorbance. The absorbances and slower kinetics of species **2** are similar to previously characterized compound **2** type species (Table 1).

Rapid mixing of ferric cyt c'_β with a 20-fold excess of mCPBA gave similar changes in both the Soret and Q-bands, but on much faster time scales than reaction with H_2O_2. During the time span of 0 to 0.02 s (Fig. 4A, red to green traces), three isosbestic points were observed at the wavelengths marked on the figure, indicating the formation of a new species (species **1′**)

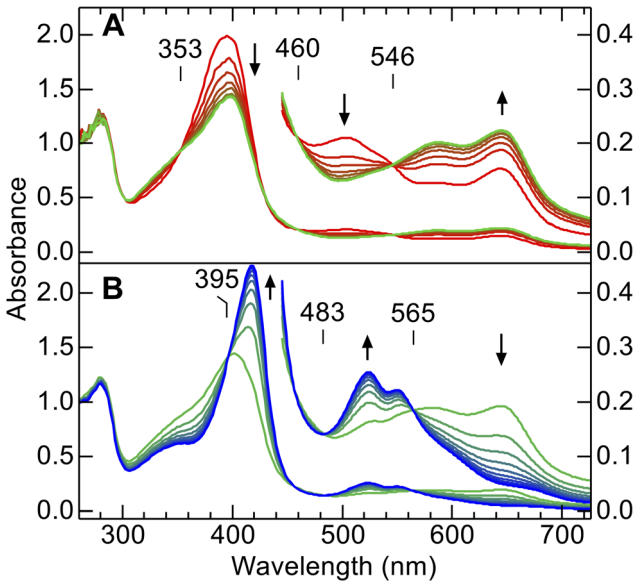

Fig. 4 Stopped-flow absorption spectra of resting cyt c'_β (40 μM) reacting with excess mCPBA (800 μM) at 4 °C in the time regimes of (A, red to green) 0 to 0.02 s and (B, green to blue) 0.5 to 20 s. The time interval between successive spectra is (A) 0.002 s and (B) 2.2 s. The insets are magnified by 5 and use the right-axis absorbance scale. The arrows indicate increasing time changes and the denoted wavelengths are isosbestic points.

concomitantly with the loss of the ferric enzyme. The equal time interval spectra showed convergence to a species with red shifted Soret band at 400 nm and Q-bands at 586, and 645 nm. The absorbances of species **1′** are similar to species **1** and to previously characterized compound **1** type species (Table 1). Over the longer time span of 0.2 to 20 s (Fig. 4B, green to blue traces), three new isosbestic points were observed at the wavelengths marked on Fig. 4, indicating the formation of a new species (species **2′**) concomitantly with the loss of species **1′**. The equal time interval spectra showed convergence to a species with a further red shifted Soret band at 417 nm, Q-bands at 521 and 551 nm, and the loss of the 645 nm absorbance. The absorbances and slower kinetics of species **2′** were similar to species **2** and to previously characterized compound **2** type species.

The RFQ-Mössbauer data (discussed below) of cyt c'_β mixed with a 20-fold excess mCPBA gave a 75%, 25% ratio of compound **1** and ferric heme species, respectively. Assuming this same ratio for the early time domain of the SF-Abs data gave extinction coefficients for species **1′** of 93 mM^{-1} cm^{-1} at 400 nm and 15 mM^{-1} cm^{-1} at 650 nm. From these values and assuming the same extinction coefficients for **1** and **1′**, the maximum temporal accumulation of species **1** during reaction with H_2O_2 was ~30% of the overall protein concentration.

For the reaction with H_2O_2, single-valued decomposition (SVD) analysis of the spectra revealed that species **1** had a rate constant of formation of $k_1 = 2.0 \times 10^3$ M^{-1} s^{-1} and a decay constant of $k_2 = 0.06$ s^{-1}. The SVD eigenspectra agree with the experimental spectra of the species observed at 0, 3 and 50 s (Fig. S1†) which correspond to the absorption spectra of the ferric, compound **1** and **2** species, respectively. Comparison of these kinetics with previously characterized compound **1** species reveal much slower formation rates than all other peroxidases and comparable or slower decay rates compared to CPO and cyt P450 (Table 2). Although the data in this paper was collected at 4 °C, the formation rate at 25 °C is estimated to be 8×10^3 M^{-1} s^{-1} assuming a doubling for every increase in 10 °C.[28] This rate is approximately 2000 times slower than that of HRP.

For the reaction with mCPBA, the SVD analysis was somewhat hindered by the much higher formation rate. Indeed, comparison of the spectra of the fastest recorded time point (0.001 s) to the as-isolated enzyme reveal a decreased Soret intensity by ~1/3 and the presence of the 650 nm feature. These findings imply that the initial formation of species **1′** is partially within the dead-time of the stopped-flow instrument (0.001 s). Nonetheless, the SVD analysis gave a lower limit for the formation rate of compound **1** to be $k_1 \geq 8.0 \times 10^5$ M^{-1} s^{-1}, which is 400 times faster than the formation of compound **1** from H_2O_2. Again, the eigenspectra agreed with the experimental spectra of the species observed at the intermediate and long-lived times. Comparison of this rate with previously studied compound **1** species produced with mCBPA (Table 2) reveal that the rate is comparable (or faster) at 25 °C (estimated at $\geq 3.2 \times 10^6$ M^{-1} s^{-1}) to other heme enzymes. These formations rates for compound **1** species from mCPBA are near the diffusion limit. The decay kinetics of compound **1** with mCPBA ($k_2 = 0.3$ s^{-1}) was the same order of magnitude as that of H_2O_2 (0.06 s^{-1}) and comparable or slower than that of CPO and cyt P450 (Table 2).

For reaction times of mCPBA greater than 60 s, compound **2** was observed to decay to another species. Optical data collected to 250 seconds (Fig. S2†) show that compound **2** decays to an

Table 2 Pre-steady state kinetic parameters of cyt c'_β compound **1**

Enzyme (oxidant)	k_1 (M^{-1} s^{-1})	k_2 (s^{-1})	Conditions	Ref.
Cyt c'_β (H_2O_2)	2.0×10^3 (±0.4)	0.06 (±0.02)	pH 7.4, 4 °C	This work
Cyt c'_β (mCPBA)	$\geq 8.0 \times 10^5$ (±1)	0.3 (±0.1)	pH 7.4, 4 °C	This work
HRP (H_2O_2)	1.4×10^7	0.0079	pH 7, 25 °C	30 and 31
HRP (mCPBA)	3.6×10^7	0.0064	pH 7, 25 °C	29
CcP (H_2O_2)	4.5×10^7	2600	pH 6.0, 25 °C	32–34
CPO (H_2O_2)	1.5×10^6	ND	pH 2.8, 25 °C	35
CPO (peroxyacetic)	3.8×10^6	0.5	pH 4.7, 25 °C	36
P450 (mCPBA)	3.20×10^5	29.4	pH 7, 25 °C	26

optical species that was approaching that of the as-isolated ferric enzyme. Previous reports found that HRP compound **2** reacts with excess mCPBA to produce inactive enzyme.[29] It may be the case that cyt c'_β compound **2** also exhibits similar behavior with mCPBA to produce an inactive species.

EPR and Mössbauer spectroscopy

EPR and Mössbauer samples of as-isolated cyt c'_β showed spectra similar to those of previous preparations indicating that the protein was in the ferric state.[9] The EPR spectra show two ferric heme species at the same ratio among numerous enzyme preparations. Fitting the spectrum to two heme species, constrained to equal amounts, gave good agreement with the experimental spectrum shown in Fig. 5A. The two species have E/D values of 0.014 and 0.026. The equal population of the two species suggests a possible dimer-like quaternary structure which was observed in the crystal structure of cyt c'_β. A non-zero E/D value is presumably associated with an asymmetric interaction of the axial His π orbital with the iron d_{xz}/d_{yz} orbitals. Presumably, the dimeric structure causes different microenvironments of the hemes within each subunit, and hydrogen bonding differences at the axial His (or near the respective heme sites) result in two orientations of the His in solution. The Mössbauer spectrum of the ferric state is consistent with this speciation but is not as sensitive to the differences in species. The total heme concentration derived from these simulations also agreed with the concentration of the sample determined from optical absorption ($\varepsilon_{400} = 91.5\ mM^{-1}\ cm^{-1}$).

RFQ samples of cyt c'_β, mixed 1 : 1 with H_2O_2 at 4 °C were quenched in liquid ethane at 95 K. The various quench delay times gave the EPR spectra of Fig. 5B–D. The data show a progressive loss of both heme species. The dilution with H_2O_2 and packing of the quench powder lowers the protein concentration by approximately a factor of 4 in the sample tube. Accounting for this factor, the 20 ms sample (Fig. 5B) has nearly the same amount of ferric heme as the control sample. At 2 seconds, both heme species have decreased in concentration to 40% of the control sample. A radical species with a sharp signal at $g = 2$ is also present in the 2 second sample. The concentration of this radical species was determined with non-saturating microwave power at 100 K to be only 2% relative to the total heme concentration. This signal is assigned to a minority radical species, possibly from protein, which may be near the heme site but is not associated with a porphyrin radical state. Similar results were observed from two other series of RFQ preparations at times of 0.06, 1, 3, and 5 s.

The SF-Abs results of cyt c'_β mixed with H_2O_2 indicated that the ferric species initially transformed into a new intermediate species, presumably compound **1**, reaching a maximum amount of 30% of the protein concentration at 0.5 s. At later times this first intermediate transformed to a second species, assigned as compound **2**. These results are compatible with the EPR data which showed the relatively slow loss of the ferric heme species. Compound **2** species are spin $S = 1$ with a large iron zero-field splitting, resulting in an EPR silent heme. Although the SF-Abs results indicated that a significant amount of compound **1** should be present in some of the EPR samples, none of spectra of the RFQ EPR samples showed a significant $S = \frac{1}{2}$ signal that could be attributed to a compound **1** intermediate. The compound **1** intermediate of catalase exhibits an $S = 3/2$ signal near $g = 4$, but no such signal was observed in these EPR samples. At later times when the amount of compound **2** is significant, only a small amount (<5% relative to heme concentration) of a radical signal was observed in EPR spectra. The transformation of compound **1** to **2** requires an electron source which is presumed to be from the protein. The lack of a significant radical signal indicates that the ensuing protein radical is short-lived.

Our extensive work with H_2O_2 suggested that a compound **1** species should be present in moderate yield, and yet the $S = \frac{1}{2}$ EPR signal of compound **1** was for some reason undetectable. Consequently, we pursued reactions using the alternative oxidant mCPBA and switched to Mössbauer spectroscopy with ^{57}Fe enriched protein to determine which iron species were forming after loss of the precursor ferric heme species during reaction. The SF-Abs suggested that a compound **1** species could be stabilized in greater yield with mCPBA because the absorption at 645 nm in Fig. 4 was approximately twice as intense as that of Fig. 3. However, as will be shown below, mCPBA also did not give an observable compound **1** EPR signal.

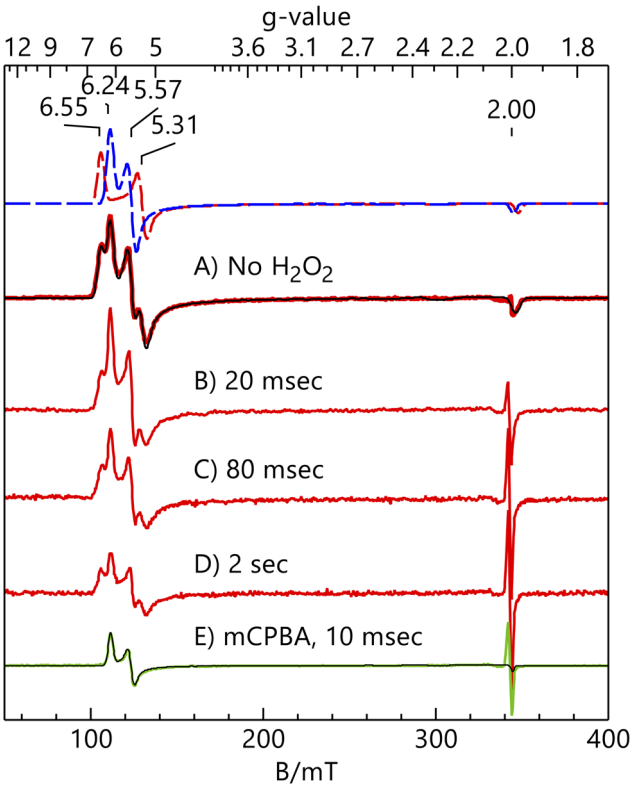

Fig. 5 X-band (9.624 GHz) EPR spectra (red traces) of as-isolated cyt c'_β (A) reacted with H_2O_2 (B–D) or mCPBA (green trace, E) at 4 °C and frozen (95 K) at the times listed. All recorded at 11 K and 0.2 mW microwave power. The simulation (black line) overlaid on the data of (A) is the sum of two species in equal amounts: $E/D = 0.014$ (blue dash), $E/D = 0.026$ (red dash).

^{57}Fe ferric cyt c'_β was mixed in equal amounts with a solution of 20 equivalents (relative to heme) of mCPBA at pH 7.4 and quenched in liquid ethane at a temperature of 95 K at reaction times of 0.01, 0.5, and 5 s. During this RFQ sample preparation, an equivalent EPR sample from the same quench powder was made of the 0.01 s time point. Upon preparation of the 0.01 s and 0.5 s samples, the reaction mixture quenched in the liquid ethane bath exhibited a striking change in color from red to green. To better understand the speciation within these samples, a separate long time point sample was prepared on the benchtop by mixing ferric cyt c'_β with 20 equivalents of mCPBA followed by freezing in liquid ethane after approximately 15 seconds. The benchtop addition gave a sample with a higher protein concentration and better signal-to-noise. The results of this long-time sample are presented next, prior to the RFQ samples, to help identify reaction species in the mixture.

The Mössbauer spectra of the 15 s sample in variable magnetic fields are shown in Fig. 6. In zero magnetic field, the spectrum (Fig. 6D) exhibited a doublet and underlying broad features typical of paramagnetic species. The doublet has an isomer shift (δ) and quadrupole splitting (ΔE_Q) indicative of an Fe^{IV}=O species (Table 3, compound **2**). In a weak magnetic field of 0.1 T, the paramagnetic species sharpen into a 6-line pattern characteristic of an $S = 5/2$ Fe^{III} species. At higher fields of 3 and 7 T, an additional minor Fe^{III} species is resolved. Fig. 6A–C shows simulations of the spectra fit to the same 3 species. The simulations are global least-squares fits of the data for the amounts and parameters given in Tables 3 and 4, respectively. The colored areas are the simulation components which sum to

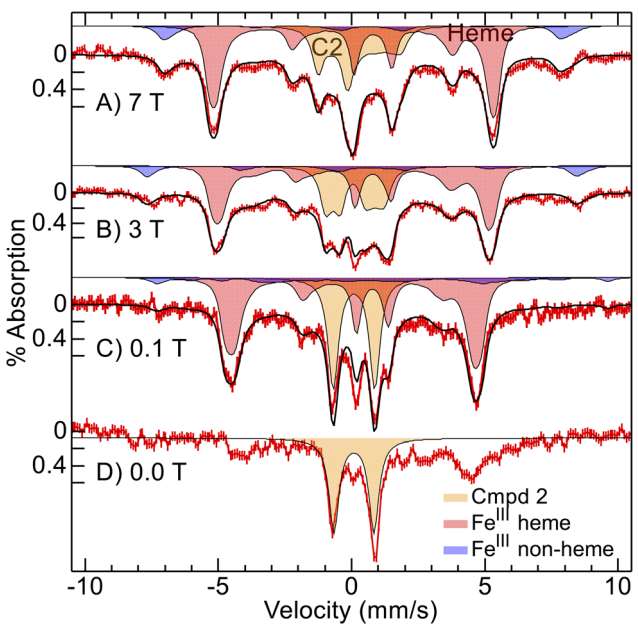

Fig. 6 ^{57}Fe Mössbauer spectra (red vertical bars) of cyt c'_β reacted with mCPBA at 4 °C and frozen (95 K) at 15 s, recorded at 4.2 K in the magnetic fields listed. The simulations (black traces) overlaid on the data are the sum of 3 species: $S = 5/2$ Fe^{III} heme (red fill), compound **2** (orange fill), and $S = 5/2$ Fe^{III} non-heme (blue fill) with amounts and parameters given in Tables 3 and 4.

Table 3 Relative absorption areas of the Mössbauer spectra produced during the reaction of cyt c'_β with mCPBA

Time (s)	% Fe^{III} heme	% Cmpd **1**	% Cmpd **2**
0.01	25	65	< 10
0.5	18	49	33
5	30		70
15[a]	57	0	31

[a] A non-heme Fe^{III} species (12%) was only observed in the 15 s sample.

give the resulting black trace overlaid on the experimental data. The majority species (red, 57%) has electronic and hyperfine parameters typical of an $S = 5/2$ Fe^{III} heme species. The first minor species (orange, 31%) has parameters indicative of an $S = 1$ Fe^{IV}=O heme and is assigned to compound **2**. The relatively low compound **2** yield is presumably caused by reduction of compound **2** at longer times from the excess equivalents of mCPBA as noted in the above SF-Abs results. The second minority species (blue, 12%) has parameters of $\delta = 0.59$ mm s^{-1}, $\Delta E_Q = 1.1$ mm s^{-1}, $D = 0.4$ cm^{-1} and $A = -21$ T which are typical of non-heme $S = 5/2$ Fe^{III} species bound adventitiously to the protein. This non-heme iron species was not observed in the RFQ samples below. The 15 s sample was from a different protein preparation than the RFQ samples, possibly some ^{57}Fe salt from the growth media was not fully exchanged out during purification. Alternatively, the longer incubation time without a substrate can cause heme degradation as has been documented in the reactions of mCPBA with HRP or cyt P450.[29,37,38]

Moving to the RFQ samples, the Mössbauer spectra of the 10 ms sample in variable magnetic fields are shown in Fig. 7. In a weak field of 45 mT oriented parallel with the gamma radiation direction, the spectrum (Fig. 7E) exhibited broad features indicative of paramagnetic species. The outer-most lines near ±5 mm s^{-1} are from unreacted Fe^{III} heme. Based on the data from Fig. 6, the inner doublet of Fig. 7E is too broad to be from the compound **2** species. Furthermore, Fig. 7D shows a spectrum in the same weak field but oriented perpendicular to the gamma ray direction. The spectra of species with an overall integer electronic spin are independent of the field orientation. The spectral change between Fig. 7D and E indicates that the majority species has half-integer spin and therefore not from compound **2**. Fig. 7 shows simulations overlaid on the experimental data which are composed of the three species: compound **1**, compound **2**, and Fe^{III} heme. The simulations are global least-squares fits of the data for the amounts and parameters given in Tables 3 and 4. There is no evidence of the adventitious non-heme Fe^{III} species in the RFQ samples. These simulations include the largest possible amount of compound **2** compatible with the data (orange, 10%). While the SF-Abs kinetics suggests that no compound **2** is present at 10 ms, we cannot rule out a 10% minority amount based on the Mössbauer data alone and is included here for completeness. The fits to the data are slightly worse by excluding compound **2**, in which case, the amount of compound **1** increases to 75%. The simulations unambiguously require that the majority features of the

Table 4 A comparison of Mössbauer parameters for compound **1** and **2** states of heme enzymes

Species	S_{Fe}	S_{Por}	δ, mm s^{-1}	ΔE_Q, mm s^{-1}	J^a, cm^{-1}	D, cm^{-1}	A, T	Ref.
Fe^{III}	5/2		0.44	+1.53		13	−19, −19, −19	This work
Cmpd **1**	1	1/2	0.08	+1.30	13	28	−25, −25, −2	This work
Cmpd **2**	1	0	0.09	+1.59		28	−22, −22, −3	This work
bCcP 1	1	1/2	0.09	+1.21	−17	28	−23, −23, −5	15
bCcP 2	1	0	0.05	+1.67		28	−23, −23, −3	15
HRP 1	1	1/2	0.08	1.25	<±4	26	−19, −19, −6	6
HRP 2	1	0	0.03	1.61		22	−19, −19, −3	39
CPO 1	1	1/2	0.14	1.02	37	36	−20, −20, −1	40
P450 1	1	1/2	0.11	0.90	47	36	−20, −23, −3	5
Catalase 1	1	1/2	0.12	1.09	−5	17	−19, −19, −6	7

[a] $H_{ex} = JS_1 \cdot S_2$.

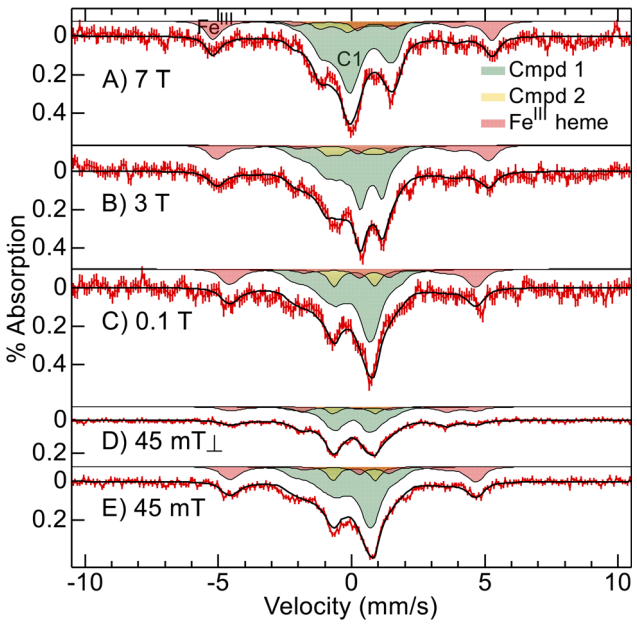

Fig. 7 ^{57}Fe Mössbauer spectra (red vertical bars) of cyt c'_β reacted with mCPBA at 4 °C and frozen (95 K) at 10 ms, recorded at 4.2 K and the magnetic fields listed. The simulations (black traces) overlaid on the data are the sum of 3 species: compound **1** (green fill), compound **2** (orange fill), and S = 5/2 Fe^{III} heme (red fill) with amounts and parameters given in Tables 3 and 4. All spectra recorded with the magnetic field parallel to the gamma ray direction, except in D where it is perpendicular.

spectra are from a compound **1** species (green, 65%). Green compound **1** species in peroxidases are composed of an $S_{Fe} = 1$ Fe^{IV}=O and a $S_{Por} = 1/2$ porphyrin π-cation radical. These spins can exchange-couple either antiferromagnetically or ferromagnetically to give a total spin state of $S = \frac{1}{2}$ or 3/2 low in energy, respectively. The exchange coupling value determined from the simulations is J = +13 cm^{-1} ($H_{ex} = JS_1 \cdot S_2$) which falls within the moderate antiferromagnetic range between the J values of HRP and CPO (Table 4).

The EPR spectrum of the equivalent 10 ms RFQ sample is shown in Fig. 5E. The spectrum shows only one of the two Fe^{III} heme species (E/D = 0.014) at an amount compatible with the Mössbauer data (25% of the heme concentration). The loss of the E/D = 0.026 heme species indicates a faster reactivity with mCPBA for this heme species. In contrast, both hemes reacted with H_2O_2 with similar but slower rates. The EPR spectrum also showed a minority radical species at g = 2. At 100 K under non-saturating microwave power, the signal quantified to 5% of the protein concentration. This minority signal may be from a nearby amino acid residue which was oxidized by compound **1**. If true, the porphyrin would have been reduced to give a compound **2** heme species, which is compatible with a minor amount of compound **2** observed in the Mössbauer spectra of

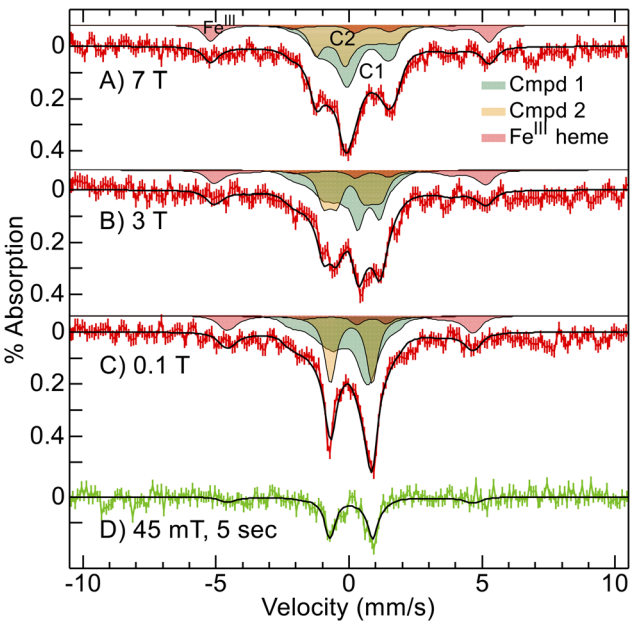

Fig. 8 ^{57}Fe Mössbauer spectra (A–C, red vertical bars) of cyt c'_β reacted with mCPBA at 4 °C and frozen (95 K) at 0.5 s, recorded at 4.2 K and the magnetic fields listed. The simulations (black traces) overlaid on the data are the sum of 3 species: compound **1** (green fill), compound **2** (orange fill), and S = 5/2 Fe^{III} heme (red fill) with amounts and parameters given in Tables 3 and 4. (D, green vertical bars) Cyt c'_β reacted with mCPBA and frozen at 5 s, with a simulation showing compound **2** and S = 5/2 Fe^{III} heme in amounts given in Table 3.

Fig. 7. Consequently, the majority of the heme in the 10 ms sample is EPR silent.

The Mössbauer spectra of the 0.5 s RFQ sample in variable magnetic fields are shown in Fig. 8A–C. In a field of 0.1 T oriented parallel to the gamma radiation direction (Fig. 8C), the spectrum exhibited a sharp doublet species which was not prominent in the 10 ms sample in the same magnetic field (Fig. 7C). The doublet is due to the presence of newly formed compound **2** species (orange, 33%). The outer-most lines at ± 5 mm s^{-1} are again attributed to $S = 5/2$ Fe^{III} heme (red, 18%). Fig. 8 show simulations overlaid on the experimental data which are composed of three species: compound **1**, compound **2**, and Fe^{III} heme. The simulations are global least-squares fits of the data with amounts and parameters given in Tables 3 and 4. The $S_{Fe} = 1$ ferryl hemes of compounds **1** and **2** have similar electronic properties, however the porphyrin is reduced ($S_{Por} = 0$) for compound **2** and thus the spectrum displays a doublet in a weak magnetic field because the lowest $m_s = 0$ level is not magnetic (orange, Fig. 8C). Whereas for compound **1**, the lowest states are paramagnetic and the species does not display a doublet (green, Fig. 8C).

The Mössbauer spectra of the 5 s RFQ sample had low absorption owing to RFQ instrumentation leakage, and therefore acquisition of high-field data was not possible. Nevertheless, the spectrum in low field (Fig. 8D) showed a doublet with values of δ and ΔE_Q matching that of compound **2**. The simulation of the spectrum gave 70% compound **2** with the remainder compatible with 30% ferric heme.

Discussion

Cytochrome cyt c'_β (cyt c'_β) from the ammonia-oxidizing bacterium *Nitrosomonas europaea* contains heme *c* (Fig. 1 and 2A).[8,9] The iron is 5-coordinate with a proximal axial His and an open distal coordination site which can bind various small ions and molecules such as cyanide and carbon monoxide. Owing to the similarity of tertiary structures, which are distinctly comprised of β-sheets, cyt c'_β is a member of the widely distributed P460 superfamily of enzymes.[10] A unique characteristic of the first characterized enzyme of the P460 superfamily, cyt P460, is an unusual cross-link connecting the 13′-meso carbon of the heme porphyrin to the nitrogen atom of a lysyl side chain of the protein backbone.[41–43] This cross-link causes a red shift in the ferrous Soret band to 460 nm.[16,44] However, c'_β possesses a Met residue (Fig. 2A) in place of the crosslinking Lys residue of cyt P460, and lacks the red-shift of the Soret band due to the absence of the cross-link in the as isolated enzyme.[9] The crystal structure of cyt c'_β confirmed the absence of the cross-link and found that the spatial position of the methionyl side chain could virtually be superimposed with the lysyl side chain of cyt P460.[8] The cross-link affects function: cyt P460 (with Lys/heme cross-link) oxidizes the substrate NH_2OH and is inactivated by H_2O_2, whereas cyt c'_β does not oxidize NH_2OH but catalytically turns over H_2O_2. *Nitrosomonas europaea* expresses both cyt P460 and cyt c'_β.[9,45] In our previous work, cyt c'_β exhibited guaiacol-dependent peroxidase activity ($k_{cat} = 20$ s^{-1}; $K_M = 2.6$ mM). The addition of a slight excess of H_2O_2 to cyt c'_β in the absence of substrate caused formation of a semistable Fe^{IV}=O compound **2** species.

The SF-Abs data of cyt c'_β reacting with H_2O_2 (Fig. 4) showed isosbestic points in the time range of 0 to 3 s with absorbances typical of compound **1** species of peroxidases (Table 1). The ferric heme reacts with H_2O_2 to produce compound **1** with a rate constant that is approximately 2000 times slower than that of HRP at the same reaction temperature. The compound **1** intermediate builds to a maximum of 30% of the total heme at ~2 s. In the later time course of 3 to 100 s, a second set of isosbestic points are observed with absorbances typical of compound **2** species of peroxidases. This later time course is the transformation of compound **1** to **2** with a decay rate of compound **1** of $k_2 = 0.06$ s^{-1}. The lifetime of compound **1** of cyt c'_β is shorter than peroxidases but longer than cyt P450 and CPO (Table 2). The slow reaction of H_2O_2 raises the possibility that the reaction with H_2O_2 could be part of a shunt mechanism, wherein the normal catalytic cycle involves O_2, with H_2O_2 being an alternative oxidant in the formation of compound-**1**.[46]

The SF-Abs data showed much faster reaction with mCPBA in comparison to H_2O_2. The species detected had similar optical features indicating that the formation of intermediates compound **1** and **2** are independent of oxidant. The presence of compound **1** and **2** were confirmed from Mössbauer spectroscopy. The data also indicated that the transformation of the ferric heme into compound **1** was nearly within the dead time of the instrument, with an estimated rate of formation $k_1 > 10^6$ M^{-1} s^{-1}. In the later time course, similar isosbestic points were detected for the transformation of compound **1** to **2**, with a decay rate of 0.3 s^{-1}. A previous study of the reaction of HRP with mCPBA gave comparable kinetics (Table 2).[29] In this previous study, mCPBA was found to cause reduction of compound **1** and **2** to Fe^{III} heme on an approximate time scale of minutes. The Mössbauer spectrum of the reaction of cyt c'_β with mCPBA after 15 s showed that a significant amount of the heme reverts back to the Fe^{III} state which is consistent with the same reduction process, but on a shorter time scale.

The distal residues to the heme in HRP, like many other peroxidases, contain a critical His/Arg pair important for movement of a proton from H_2O_2 (Fig. 2C).[1] In cyt c'_β, Arg46 is in a similar location to the His170 of HRP and forms a hydrogen bond with a heme propionate group, but cyt c'_β lacks the corresponding His residue of the His/Arg pair. This suggests that Arg46 is a critical catalytic residue in cyt c'_β, and could be akin to the *b*-type heme DyP peroxidases where a conserved distal Arg serves to transfer the proton from the proximal to the distal oxygen of the peroxide during O–O excision.[47,48] We find that the rate (k_1) of compound **1** formation in cyt c'_β is approximately 2000 times slower than typical peroxidases. However, the reaction with mCPBA at pH 7.4 gave a compound **1** formation rate more than 400 times faster than with H_2O_2, with a rate that is comparable to other peroxidases which approach the diffusion limit. The recovery of the fast formation rate is likely due to the lower pK_a of mCPBA (7.6) relative to H_2O_2 (11.6). For the pH 7.4 reaction conditions of our study, the amount of deprotonated mCPBA would be ~10 equivalents relative to heme and when bound to the iron could be charge stabilized by the cationic Arg

side chain. Owing to the lower pK_a of mCPBA relative to that of H_2O_2, the fraction of deprotonated acid is large such that there is no assistance needed for deprotonation. The O–O bond scission for this pathway can immediately proceed to form compound **1** and thus a much faster formation rate compared to H_2O_2. Elevated reaction rates with mCPBA over H_2O_2 have been observed previously in other heme enzymes and heme model complexes.[3,25]

Electronic properties of compound 1

In the short time span after reaction of cyt c'_β with H_2O_2 or mCPBA, the green color and similarity of optical spectra with HRP indicate the presence of a porphyrin radical. The Mössbauer data for both enzymes indicate the presence of a $S_{Fe} = 1$ Fe^{IV}=O center which is exchange coupled to a porphyrin $S_{Por} = 1/2$ radical species. The magnetic properties of compound **1** heme species have a rich history in association with their electronic structures. The classic cases are the heme *b* enzymes eukaryotic cytochrome *c* peroxidase (CcP) and HRP where compound **1** is composed of spin $S_{Fe} = 1$ Fe^{IV}=O and a spin $S = 1/2$ center which is located either on a protein radical (Trp in CcP) or as a porphyrin radical (HRP). In CcP, the weak exchange interaction between the heme iron and the Trp radical is mediated by an Asp residue, $J \sim 0.1$ cm^{-1},[49,50] which broadens the Trp radical signal but is readily detectable.[51] For HRP, the exchange interaction complicated the detection of the EPR signal. Early in the history of HRP, compound **1** was known to be two oxidation equivalents above the ferric state and thus an overall half-integer spin. However, the identification of the HRP $S = 1/2$ EPR signal came sometime later because the exchange coupling constant is larger than that of CcP and causes significant broadening of the EPR signal.[6,52,53] This complication in studies of HRP is pertinent to the present work. For cyt c'_β, multiple RFQ samples gave no evidence of a broader HRP-like $g = 2$ EPR signal or any other signal attributable to compound **1**, even though the SF-Abs data indicated that significant amounts of a compound **1** species were produced. The reason for the absence of an EPR signal attributable to the c'_β compound **1** species is discussed next.

For an exchange interaction which is large compared to the zero-field splitting energy ($|J| \gg |D|$), the $S_{Fe} = 1$ and $S_{Por} = 1/2$ spins are coupled to give total spin states of $S = 1/2$ and 3/2 which are simple to model as isolated pairs of $m_s = \pm 1/2$ states for EPR spectra. However, the iron of ferryl hemes has large zero-field splitting energies (+20 to +40 cm^{-1}, Table 4). For $J \leq D$, as is the case here, the $S = 1/2$ and 3/2 spin states are mixed causing the spin expectation at the iron and the experimentally observed g-tensor (g_{eff}) to be strongly dependent on the ratio J/D.[40] For an antiferromagnetic exchange constant ($J > 0$, $S = 1/2$ lowest in energy), as J/D increases from zero, the $g_{eff,\perp}$ value passes from 2.0 ($J/D = 0$) through 0 ($J/D = 0.4$) to 1.6 ($J/D = 1$) and >2.0 ($J/D > 1.3$). For HRP with $|J/D| \approx 0.1$, the values of the g_{eff}-tensor are all near 2 and the spectrum is broad owing to the spin interaction. For chloroperoxidase (CPO) with $J/D \approx 1$, the $S = 1/2$ signal is nearly axial with $g_{eff,\perp} = 1.73$. The variable field Mössbauer data for c'_β allowed determination of both J and D to give $J/D = 0.46$ (Table 4). This value of J/D gives $g_{eff,\perp} = 0.28$ and the predicted X-band EPR spectrum spans more than 3 T (Fig. S3†). The spectral linewidth at this g-value is dominated by a distribution of values in either D or J. The simulation uses $\sigma_D = 1$ cm^{-1}, which is small in comparison to the value of $D = 28$ cm^{-1}. The $g_{eff,\perp}$ value is dependent on the intrinsic $g_\perp$-value of the ferryl iron, assumed to be 2.21. This was the intrinsic $g_\perp$-value experimentally determined for bCcP;[15] very few of these values are known but variations in the value will not significantly change the results here. The combination of low transition probability and large overall linewidth results in a vanishingly small intensity for the signal. The feature at $g = 2$ in Fig. S3† is sharp but may be further broadened by hyperfine interactions or anisotropy in the porphyrin radical *g*-tensor. Nevertheless, the feature is overwhelmed by a minority radical signal from an unknown source. For the intensity of the EPR signal to be above this minority radical signal, or the noise in the spectrum at higher field, would require a 200-fold increase in enzyme concentration, which is why no EPR signal was detected from compound **1** of cyt c'_β in our studies.

Green compound **1** species have an Fe^{IV}=O center with an intermediate spin $S_{Fe} = 1$ state and an electronic configuration for the iron t_{2g} orbitals of $d_{xy_2}d_{xz_1}d_{yz_1}$. The porphyrin π-orbital containing the unpaired spin ($S_{Por} = 1/2$) is either a_{1u} or a_{2u} symmetry in idealized D_{4h} symmetry. The two spins are exchange coupled but since the iron and porphyrin orbitals containing the unpaired electrons have different inversion symmetry the exchange-coupling constant is relatively small, $|J| < 50$ cm^{-1} ($H_{ex} = JS_1 \cdot S_2$). The oxidation reactions that enzymes with heme *b* catalyze are dependent on the heme environment and the identity of the axial heme ligand, of which examples are: S-Cys (cyt P450), N-His (HRP), and O-Tyr (catalase). The variation of the value of J has also been observed to be correlated with the heme axial ligand. The value of J is antiferromagnetic ($J > 0$) for cyt P450, near zero for HRP, and ferromagnetic ($J < 0$) for catalase.[5–7]

The exchange coupling constant (J) for cyt c'_β was found to be significantly different than that of all other compound **1** species (Table 4). Cyt c'_β, bCcP and HRP exhibit significantly different exchange constants with other comparable electronic parameters, despite all three containing an axial N-donor to the heme. The isomer shift, quadrupole splitting, and D-value of compound **1** in cyt c'_β bCcP and HRP are all similar, but differ significantly from those of CPO, P450 and catalase (Table 4), suggesting that these values are primarily influenced by the axial ligand to the heme iron. The orientation of the axial His is a distinct structural difference associated with heme *b versus* heme *c*. The CXXCH peptide chain for cyt c'_β and bCcP causes a rotation of greater than 90° of the imidazole/His plane relative to that of HRP. The relevant dihedral angle is defined in Fig. 2 and for these structures is: 55° (cyt c'_β), 41° (bCcP), 169° (HRP). However, this angle is approximately the same for cyt c'_β and bCcP and yet the exchange constant is different by 30 cm^{-1} and with a sign change. The large change in the exchange constant between cyt c'_β and bCcP, and relative to HRP, also does not indicate a specific dependence on *c*-type *versus b*-type hemes.

Owing to the different inversion symmetry of the iron and porphyrin orbitals with the unpaired electrons, the exchange constant is expected to be ferromagnetic ($J < 0$) in accordance with the Goodenough–Kanamori rules.[54,55] Consequently, the antiferromagnetic exchange constant ($J > 0$) for cyt P450 and CPO has been suggested to require delocalization of the porphyrin radical onto the axial sulfur atom,[17–21] which could also influence enzymatic function. However, ENDOR studies of CPO compound **1** found relatively little spin density on the axial sulfur.[56] Like for cyt P450 and CPO, the exchange constant for cyt c'_β is antiferromagnetic ($J = +13$ cm^{-1}). The propensity to delocalize spin density onto the His axial heme ligand is no different for cyt c'_β bCcP or HRP, indicating that an antiferromagnetic exchange constant does not require spin localization onto the axial ligand. The change in the value of J between bCcP and cyt c'_β is 30 cm^{-1}, which is similar to the change in the value of J between cyt c'_β and CPO (Table 4). These observations suggest that structural properties other than the axial ligand or heme type are important in influencing the exchange constant. For example, hydrogen bonding to the heme propionates has been suggested to influence the electronic structure of the heme and the stabilization of a porphyrin radical.[57,58] Also, a propionate in cyt c'_β hydrogen bonds to the proximal His which may contribute to the observed heme distortion. Further computational work is ongoing to examine how changes in electronic structure induced by propionate hydrogen bonds and/or heme distortions may be responsible for the observed variation in the exchange constant.

Conclusion

A compound **1** intermediate has been detected from a second enzyme containing heme *c* indicating that the formation of compound **1** is not confined to cytochromes with heme *b*. Like HRP, cyt c'_β and bCcP have an axial His ligand and many of the electronic properties of the compound **1** states of these enzymes are similar. However, the exchange coupling constant for compound **1** of the three enzymes differ significantly indicating that the exchange constant is not dominated or solely dependent on the axial ligand to the heme or heme type.

Nitrosomonas europaea expresses superoxide dismutase, which produces H_2O_2 from superoxide radicals likely generated during its metabolic use of ammonia and oxygen.[9] To remove H_2O_2, *Nitrosomonas europaea* utilizes catalase and peroxidases (*e.g.* bCcP). Thus, the slow reaction rate of cyt c'_β with H_2O_2 and the presence of catalase and other peroxidases suggests that the *in vivo* function of cyt c'_β is not directed solely at the removal of H_2O_2, and possibly the reaction of the ferric enzyme with H_2O_2 is part of a shunt mechanism. Nevertheless, the presence of a long-lived compound **1** indicates an obligate catalytic intermediate in the function of the enzyme. The protein environment near the active site of cyt c'_β protects against deleterious side reactions thereby facilitating reactions of compound **1** towards cellular substrates. The presence of cyt c'_β in an ammonia-oxidizing bacterium suggests a function involving oxidation of nitrogen containing substrates. Work is ongoing to identify the *in vivo* substrate and the corresponding catalytic cycle.

Materials and methods

The ESI contains experimental methods, spectroscopic methods, SVD comparisons, and ESI figures.†

Data availability

All study data are included in the article and/or ESI.†

Author contributions

MH and JP wrote the manuscript. MH designed the experiments. JN and HK performed protein expression, purification, isotope incorporation; reviewed and edited manuscript. MH and JP performed the experiments and analyzed the data.

Conflicts of interest

There are no conflicts of interest to report.

Acknowledgements

The authors acknowledge the NIH (GM141948 to M. P. H.) and the University of Washington SRCP and startup (to H. J. K.) for funding.

References

1 T. L. Poulos, *Chem. Rev.*, 2014, **114**, 3919–3962.
2 P. C. E. Moody and E. L. Raven, *Acc. Chem. Res.*, 2018, **51**, 427–435, DOI: **10.1021/acs.accounts.7b00463**.
3 X. Huang and J. T. Groves, *Chem. Rev.*, 2018, **118**, 2491–2553, DOI: **10.1021/acs.chemrev.7b00373**.
4 H. J. Kim, O. Khalimonchuk, P. M. Smith and D. R. Winge, *Biochim. Biophys. Acta*, 2012, **1823**, 1604–1616, DOI: **10.1016/j.bbamcr.2012.04.008**.
5 J. Rittle and M. T. Green, *Science*, 2010, **330**, 933–937, DOI: **10.1126/science.1193478**.
6 C. E. Schulz, P. W. Devaney, H. Winkler, P. G. Debrunner, N. Doan, R. Chiang, R. Rutter and L. P. Hager, *FEBS Lett.*, 1979, **103**, 102–105.
7 O. Horner, J. M. Mouesca, P. L. Solari, M. Orio, J. L. Oddou, P. Bonville and H. M. Jouve, *J. Biol. Inorg. Chem.*, 2007, **12**, 509–525, DOI: **10.1007/s00775-006-0203-9**.
8 J. Abendroth, G. W. Buchko, F. N. Liew, J. N. Nguyen and H. J. Kim, *Biochemistry*, 2022, **61**, 563–574, DOI: **10.1021/acs.biochem.1c00640**.
9 F. N. Liew, M. A. Brandys, S. Biswas, J. N. Nguyen, M. Rahmawati, M. Nevala, B. O. Elmore, M. P. Hendrich and H. J. Kim, *Biochemistry*, 2020, **59**, 704–716, DOI: **10.1021/acs.biochem.9b00810**.
10 B. O. Elmore, D. J. Bergmann, M. G. Klotz and A. B. Hooper, *FEBS Lett.*, 2007, **581**, 911–916, DOI: **10.1016/j.febslet.2007.01.068**.

11 G. I. Berglund, G. H. Carlsson, A. T. Smith, H. Szoke, A. Henriksen and J. Hajdu, *Nature*, 2002, **417**, 463–468, DOI: 10.1038/417463a.
12 V. Yin, G. S. Shaw and L. Konermann, *J. Am. Chem. Soc.*, 2017, **139**, 15701–15709, DOI: 10.1021/jacs.7b07106.
13 A. Mandal, C. L. Hoop, M. DeLucia, R. Kodali, V. E. Kagan, J. Ahn and P. C. van der Wel, *Biophys. J.*, 2015, **109**, 1873–1884, DOI: 10.1016/j.bpj.2015.09.016.
14 H. Shimizu, D. J. Schuller, W. N. Lanzilotta, M. Sundaramoorthy, D. M. Arciero, A. B. Hooper and T. L. Poulos, *Biochemistry*, 2001, **40**, 13483–13490.
15 P. Hewitt, M. P. Hendrich and S. J. Elliott, *Chem. Sci.*, 2025, **16**, 6070–6078, DOI: 10.1039/d4sc07339h.
16 M. M. Bollmeyer, R. E. Coleman, S. H. Majer, S. D. Ferrao and K. M. Lancaster, *J. Am. Chem. Soc.*, 2023, **145**, 14404–14416.
17 R. Weiss, D. Mandon, T. Wolter, A. X. Trautwein, M. Muther, E. Bill, A. Gold, K. Jayaraj and J. Terner, *JBIC, J. Biol. Inorg. Chem.*, 1996, **1**, 377–383, DOI: 10.1007/s007750050069.
18 M. Shoji, H. Isobe, T. Saito, Y. Kitagawa, S. Yamanaka, T. Kawakami, M. Okumura and K. Yamaguchi, *Int. J. Quantum Chem.*, 2008, **108**, 2950–2965, DOI: 10.1002/qua.21868.
19 J. C. Schoneboom, F. Neese and W. Thiel, *J. Am. Chem. Soc.*, 2005, **127**, 5840–5853, DOI: 10.1021/ja0424732.
20 M. T. Green, *J. Am. Chem. Soc.*, 2000, **122**, 9495–9499, DOI: 10.1021/ja994377k.
21 M. T. Green, *J. Am. Chem. Soc.*, 2001, **123**, 9218–9219, DOI: 10.1021/Ja010105h.
22 W. E. Blumberg, J. Peisach, B. A. Wittenberg and J. B. Wittenberg, *J. Biol. Chem.*, 1968, **243**, 1854–1862.
23 R. Rutter, M. Valentine, M. P. Hendrich, L. P. Hager and P. G. Debrunner, *Biochemistry*, 1983, **22**, 4769–4774.
24 D. M. Davies, P. Jones and D. Mantle, *Biochem. J.*, 1976, **157**, 247–253, DOI: 10.1042/bj1570247.
25 M. M. Palcic, R. Rutter, T. Araiso, L. P. Hager and H. B. Dunford, *Biochem. Biophys. Res. Commun.*, 1980, **94**, 1123–1127, DOI: 10.1016/0006-291x(80)90535-5.
26 D. G. Kellner, S.-C. Hung, K. E. Weiss and S. G. Sligar, *J. Biol. Chem.*, 2002, **277**, 9641–9644, DOI: 10.1074/jbc.C100745200.
27 J. Rittle, J. M. Younker and M. T. Green, *Inorg. Chem.*, 2010, **49**, 3610–3617.
28 J. H. Espenson, *Chemical Kinetics and Reaction Mechanisms*, McGraw-Hill, Inc., New York, 2nd edn, 1995.
29 J. N. Rodriguez-Lopez, J. Hernández-Ruiz, F. Garcia-Cánovas, R. N. Thorneley, M. Acosta and M. B. Arnao, *J. Biol. Chem.*, 1997, **272**, 5469–5476, DOI: 10.1074/jbc.272.9.5469.
30 A. T. Smith, S. A. Sanders, R. N. Thorneley, J. F. Burke and R. R. Bray, *Eur. J. Biochem.*, 1992, **207**, 507–519.
31 M. B. Arnao, M. Acosta, J. A. del Rio, R. Varon and F. Garcia-Canovas, *Biochim. Biophys. Acta*, 1990, **1041**, 43–47.
32 S. Loo and J. E. Erman, *Biochemistry*, 1975, **14**, 3467–3470, DOI: 10.1021/bi00686a027.
33 T. Yonetani and G. S. Ray, *J. Biol. Chem.*, 1965, **240**, 4503, DOI: 10.1016/S0021-9258(18)97090-0.
34 M. Chance, L. Powers, T. Poulos and B. Chance, *Biochemistry*, 1986, **25**, 1266–1270.
35 J. A. Thomas, D. R. Morris and L. P. Hager, *J. Biol. Chem.*, 1970, **245**, 3135–3142, DOI: 10.1016/s0021-9258(18)63033-9.
36 T. Araiso, R. Rutter, M. M. Palcic, L. P. Hager and H. B. Dunford, *Can. J. Biochem.*, 1981, **59**, 233–236.
37 A. N. Hiner, J. Hernandez-Ruiz, F. Garcia-Canovas, A. T. Smith, M. B. Arnao and M. Acosta, *Eur. J. Biochem.*, 1995, **234**, 506–512, DOI: 10.1111/j.1432-1033.1995.506_b.x.
38 T. Spolitak, J. H. Dawson and D. P. Ballou, *J. Biol. Chem.*, 2005, **280**, 20300–20309, DOI: 10.1074/jbc.M501761200.
39 C. Schulz, R. Chiang and P. G. Debrunner, *J. Phys.*, 1979, **40**, 534–536.
40 R. Rutter, L. P. Hager, H. Dhonau, M. Hendrich, M. Valentine and P. Debrunner, *Biochemistry*, 1984, **23**, 6809–6816.
41 D. J. Bergmann and A. B. Hooper, *FEBS Lett.*, 1994, **353**, 324–326.
42 D. M. Arciero and A. B. Hooper, *FEBS Lett.*, 1997, **410**, 457–460.
43 A. R. Pearson, B. O. Elmore, C. Yang, J. D. Ferrara, A. B. Hooper and C. M. Wilmot, *Biochemistry*, 2007, **46**, 8340–8349.
44 D. J. Bergmann and A. B. Hooper, *Eur. J. Biochem.*, 2003, **270**, 1935–1941.
45 J. K. Zorz, J. A. Kozlowski, L. Y. Stein, M. Strous and M. Kleiner, *Front. Microbiol.*, 2018, **9**, 938.
46 I. G. Denisov, T. M. Makris, S. G. Sligar and I. Schlichting, *Chem. Rev.*, 2005, **105**, 2253–2278, DOI: 10.1021/cr0307143.
47 R. Singh, J. C. Grigg, Z. Armstrong, M. E. P. Murphy and L. D. Eltis, *J. Biol. Chem.*, 2012, **287**, 10623–10630, DOI: 10.1074/jbc.M111.332171.
48 J. N. Roberts, R. Singh, J. C. Grigg, M. E. P. Murphy, T. D. H. Bugg and L. D. Eltis, *Biochemistry*, 2011, **50**, 5108–5119.
49 A. L. P. Houseman, P. E. Doan, D. B. Goodwin and B. M. Hoffman, *Biochemistry*, 1993, **32**, 4430–4443.
50 J. E. Huyett, P. E. Doan, R. Gurbiel, A. L. P. Houseman, M. Sivaraja, D. B. Goodin and B. M. Hoffman, *J. Am. Chem. Soc.*, 1995, **117**, 9033–9041, DOI: 10.1021/ja00140a021.
51 T. Yonetani, H. Yamamoto, J. E. Erman, J. S. Leigh Jr and G. H. Reed, *J. Biol. Chem.*, 1972, **247**, 2447–2455.
52 J. E. Roberts, B. M. Hoffman, R. Rutter and L. P. Hager, *J. Am. Chem. Soc.*, 1981, **103**, 7654–7656.
53 J. E. Roberts, B. M. Hoffman, R. Rutter and L. P. Hager, *J. Biol. Chem.*, 1981, **256**, 2118–2121.
54 J. B. Goodenough, *J. Phys. Chem. Solids*, 1958, **6**, 287–297, DOI: 10.1016/0022-3697(58)90107-0.
55 J. Kanamori, *J. Phys. Chem. Solids*, 1959, **10**, 87–98, DOI: 10.1016/0022-3697(59)90061-7.
56 S. H. Kim, R. Perera, L. P. Hager, J. H. Dawson and B. M. Hoffman, *J. Am. Chem. Soc.*, 2006, **128**, 5598–5599, DOI: 10.1021/ja060776l.
57 V. Guallar, M.-H. Baik, S. J. Lippard and R. A. Friesner, *Proc. Natl. Acad. Sci. U. S. A.*, 2003, **100**, 6998–7002.
58 T. P. Barrows and T. L. Poulos, *Biochemistry*, 2005, **44**, 14062–14068.